EUROPEAN ORGANIZATION FOR NUCLEAR RESEARCH

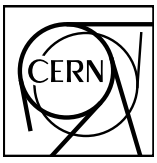

CERN-EP-2016-xxx
5 December 2016

Systematic studies of correlations between different order flow harmonics in Pb–Pb collisions at $\sqrt{s_{\rm NN}} = 2.76$ TeV

ALICE Collaboration *

Abstract

The correlations between event-by-event fluctuations of amplitudes of anisotropic flow harmonics have been measured in Pb–Pb collisions at $\sqrt{s_{\rm NN}} = 2.76$ TeV with the ALICE detector at the Large Hadron Collider. The results were obtained with the multi-particle ~~cumulant method~~ correlation observables dubbed symmetric cumulants. ~~This method is~~ These observables are robust against systematic biases originating from non-flow effects. The centrality dependence of correlation between the higher order harmonics (v_3, v_4 and v_5) and the lower order harmonics (v_2 and v_3) as well as the transverse momentum dependence of correlations of v_3 ~~-v_2 and~~ and v_2, v_4 ~~-~~and v_2 correlations are presented. The results are compared to calculations from viscous hydrodynamics and A Multi-Phase Transport (AMPT) ~~models. The comparisons~~ model calculations. The comparison to viscous hydrodynamic ~~models demonstrate~~ model demonstrates that the different order harmonic correlations respond differently to the initial conditions or the temperature dependence of the shear viscosity to the entropy density ratio (η/s). The small η/s regardless of initial conditions is favored and the small η/s with the AMPT initial condition is closest to the measurements. ~~v_3-~~Correlations between v_2, v_3 and v_4 ~~-v_2 correlations~~ magnitudes show moderate $p_{\rm T}$ dependence in mid-central collisions. This might be an indication of possible viscous corrections for the equilibrium distribution at hadronic freeze-out, which might help to understand possible contribution of bulk viscosity in a hadronic phase of the system. Together with the existing measurements of individual flow harmonics the presented results provide further constraints on initial conditions and the transport properties of the system produced in heavy-ion collisions.

*See Appendix A for the list of collaboration members

1 Introduction

The main emphasis of the ultra-relativistic heavy-ion collisions at the Relativistic Heavy Ion Collider (RHIC) and the Large Hadron Collider (LHC) is to study deconfined phase of the strongly interacting nuclear matter, the Quark-Gluon Plasma (QGP). This matter exhibits strong collective and anisotropic flow in the plane transverse to the beam direction, which is driven by the anisotropic pressure gradients, resulting in more particles emitted in the direction of the largest gradients. The large elliptic flow discovered at RHIC energies [**?**] continues to increase also at LHC energies [**? ?**]. This has been predicted by calculations utilizing viscous hydrodynamics [**? ? ? ? ? ?**]. These calculations also demonstrated that the shear viscosity to the entropy density ratio (η/s) of QGP is close to a universal lower bound $1/4\pi$ [**?**] in heavy-ion collisions at RHIC and LHC energies.

The temperature dependence of the η/s has some generic features that most of the known fluids obey. For instance, one such general behavior is that the ratio typically reaches its minimum value close to the phase transition region [**?**]. It was shown, using kinetic theory and quantum mechanical considerations [**?**], that $\eta/s \sim 0.1$ would be the correct order of magnitude for the lowest possible shear viscosity to entropy ratio value found in nature. Later it was demonstrated that an exact lower bound $(\eta/s)_{\rm min} = 1/4\pi \approx 0.08$ can be calculated using the AdS/CFT correspondence [**?**]. Hydrodynamical simulations support as well the view that η/s of the QGP matter is close to that limit [**?**]. This ~~in turn~~ may have important implications for other fundamental physics goals. It is argued that such a low value might imply that thermodynamic trajectories for the expanding matter would lie close to the quantum chromodynamics (QCD) critical end point, which is another subject of intensive experimental quest ~~[?]~~[**? ?**].

Anisotropic flow [**?**] is traditionally quantified with ~~harmonics~~ $n^{\rm th}$-order flow coefficients v_n and corresponding symmetry plane angles Ψ_n in the Fourier ~~series~~ decomposition of particle azimuthal distribution in the plane transverse to the beam direction [**?**]:

$$E\frac{{\rm d}^3N}{{\rm d}p^3} = \frac{1}{2\pi}\frac{{\rm d}^2N}{p_{\rm T}{\rm d}p_{\rm T}{\rm d}\eta}\left\{1+2\sum_{n=1}^{\infty} v_n(p_{\rm T},\eta)\cos[n(\varphi-\Psi_n)]\right\}, \quad (1)$$

where E, ~~N,~~ p, $p_{\rm T}$, φ and η are the ~~energy, particle yield, total~~ particle's energy, momentum, transverse momentum, azimuthal angle and pseudorapidity~~of particles~~, respectively, and Ψ_n is the azimuthal angle of the symmetry plane of the $n^{\rm th}$-order harmonic. ~~The $n^{\rm th}$-order flow coefficients are denoted as~~ v_n ~~and~~ can be calculated as $v_n = \langle\cos[n(\varphi-\Psi_n)]\rangle$, where the brackets denote an average over all particles in all events. The anisotropic flow in heavy-ion collisions is understood as hydrodynamic response of produced matter to spatial deformations of the initial energy density profile [**?**]. This profile fluctuates event-by-event due to ~~fluctuations of the positions of the~~ fluctuating position of the constituents inside the colliding nuclei, which ~~in turn implies that the flow~~ implies that v_n also fluctuates [**? ?**]. The recognition of the importance of flow fluctuations ~~has~~ led to triangular ~~flow~~ and higher flow harmonics [**? ?**] as well as ~~the correlations between different Fourier~~ to the correlation between different v_n harmonics [**? ?**]. The higher order harmonics are expected to be ~~particularly~~ sensitive to fluctuations in the initial conditions and to the magnitude of η/s [**? ?**], while v_n correlations have the potential to discriminate ~~the~~ between these two respective contributions~~to anisotropic flow development~~ [**?**]. ~~And the v_n distributions carry detailed information about the initial energy density profile [? ?].~~

~~However, difficulties on~~ Difficulties in extracting η/s in heavy-ion collisions can be attributed mostly to the fact that it strongly depends on the specific choice of the initial conditions [**? ? ?**]. The viscous effects reduce the magnitude of the elliptic flow. Furthermore, the magnitude of η/s used in ~~these~~ hydrodynamic calculations should be considered as an average over the temperature ~~history~~ evolution of the expanding fireball as it is known that η/s of other fluids depends on temperature. In addition, part of the elliptic flow can also originate from the hadronic phase [**? ? ?**]. Therefore, knowledge of both the temperature dependence of η/s and the relative contributions from the partonic and hadronic phases

should be understood better to quantify η/s of the partonic fluid.

An important input to the hydrodynamic model simulations is the distribution of energy density in the transverse plane (the initial density profile), which is usually estimated from the probability distribution of nucleons in the incoming nuclei. This initial energy density profile can be quantified by calculating the distribution of the spatial eccentricity [**?**],

$$\varepsilon_n e^{in\Phi_n} = -\{r^n e^{in\phi}\}/\{r^n\}, \tag{2}$$

where the curly brackets denote the average over the transverse plane, i.e., $\{\cdots\} = \int dxdy\ e(x,y,\tau_0)\ (\cdots)$, r is the distance to the system's center of mass~~from nucleon position~~, $e(x,y,\tau_0)$ is the energy density at the initial time τ_0, and Φ_n is the participant plane angle (see Ref. [**?** **?**]). There are experimental and theoretical evidences [**?** **?** **?**] that the harmonic coefficients, v_2 and v_3, are to a good approximation linearly proportional to the deformations in the initial energy density in the transverse plane (e.g. $v_n \propto \varepsilon_n$ for n=2 or 3). v_4 and higher order flow coefficients can arise from initial anisotropies in the same harmonic [**?** **?** **?** **?**] (linear response) or can be induced by lower-order harmonics [**?** **?**] (nonlinear response). ~~Therefore the~~ The higher harmonics ($n > 3$) could be understood as superpositions of linear and nonlinear responses, through which they are correlated with lower order harmonics [**?** **?** **?** **?**]. When the order of harmonic is large, the nonlinear response contribution in viscous hydrodynamics is dominant and become larger for more peripheral collisions [**?** **?**]. The magnitude of the viscous corrections as a function of p_{T} for v_4 and v_5 is sensitive to ansatz used for the viscous distribution function, a correction for the equilibrium distribution at hadronic freeze-out [**?** **?**]. Hence the studies of the higher order ($n > 3$) to lower order (v_2 or v_3) harmonic correlations and their p_{T} dependence can help to understand the viscous correction to the momentum distribution at hadronic freeze-out which is ~~probably~~ among the least understood part of hydrodynamic calculations [**?** **?**].

Recently, ALICE Collaboration measured for the first time the new multiparticle observables, the Symmetric 2-harmonic 4-particle Cumulants (SC), which quantify the relationship between event-by-event fluctuations of two different flow harmonics [**?**]. The new observables are particularly robust against few-particle non-flow correlations and they provide ~~orthogonal~~ independent information to recently analyzed symmetry plane correlators. It was demonstrated that they are sensitive to the temperature dependence of η/s of the expanding medium and therefore simultaneous descriptions of different order harmonic correlations would constrain both the initial conditions and the medium properties [**?** **?**]. In this article, we have extended ~~that analysis~~ the analysis of SC observables to higher order Fourier ~~harmonic~~ harmonics (up to 5$^{\mathrm{th}}$ order) ~~correlations~~ as well as to p_{T} dependence of correlations for the lower order harmonics (v_3-v_2 and v_4-v_2). We also include extensive ~~comparisons~~ comparison to hydrodynamic and AMPT model calculations. In Sec. 2 we summarize our findings from the previous work [**?**] and present the analysis methods. The experimental setting and measurements are described in Sec. 3 and the sources of systematic uncertainties are explained in Sec. 4. ~~Various theoretical models used in the article are described in Sec. ??.~~ The results of the measurements are presented in Sec. 5. In Sec. 6 we present comparisons to theoretical calculations. Various theoretical models used in the article are described in Sec. 6. Sec. 7 summarizes our findings.

2 ~~Data Analysis~~Experimental Observables

2.1 ~~Experimental Observables~~

~~While from existing measurements an estimate can be placed on~~ The existing measurements provide an estimate of the average value of QGP's η/s, both at RHIC and LHC energies~~, what remains completely unknown~~. What remains uncertain is how the η/s of QGP depends on temperature (T). ~~This study~~ The temperature dependence of η/s in the QGP was discussed in [**?**]. The effects to hadron spectra and elliptic flow were studied in [**?**] for different parametrizations of $\eta/s(T)$. A more systematic

study with the event-by-event EKRT+viscous hydrodynamic calculations has been just initiated ~~by the theorists~~ in Ref. [**?**], where the first (and only rather qualitative) possibilities where investigated (see Fig. 1 therein). The emerging ~~consensus of late is that it is unlikely that~~ picture is that the study of individual flow harmonics v_n will unlikely reveal the details of $\eta/s(T)$ dependence. ~~In fact, in~~ It was demonstrated already in ~~the initial study~~ [**?**] that different $\eta/s(T)$ parameterizations can lead to the same centrality dependence of individual flow harmonics. In Ref. [**?**] new flow observables were introduced ~~by the theorists,~~ which quantify the degree of correlation between two different harmonics v_m and v_n. ~~The initial success of these new observables was attributed to their~~ These new observables have potential to discriminate ~~for the first time the two respective~~ the contributions to anisotropic flow ~~development—from~~ development from initial conditions and from the transport properties of the QGP [**?**]. Therefore their measurements ~~in turn would enable the experimental verification of~~ would provide the experimental constrains of the theoretical predictions for individual stages of heavy-ion evolution independently. ~~Besides this advantage~~In addition, it turned out that correlations of different flow harmonics are sensitive to the ~~details of $\eta/s(T)$ dependence~~ temperature dependence of η/s [**?**], to which individual flow harmonics are ~~nearly insensitive~~weakly sensitive [**?**].

For ~~technical reasons , discussed in detail in Refs.~~ reasons discussed in [**?** **?**], the correlations between different flow harmonics cannot be studied experimentally with the same set of observables introduced ~~by the theorists in Ref. [**?**]. Instead, in [**?**]~~in [**?**]. Based on [**?**], the new flow observables obtained from multiparticle correlations, so-called *Symmetric Cumulants (SC)*, were introduced~~to quantify in the most reliable way (i. e. ~~ . SC observables are nearly insensitive to nonflow ~~)~~ and quantify the correlation of amplitudes of two different flow harmonics. The ~~technical details are elaborated in Ref. [**?**], while the~~ first measurements of SC observables were recently ~~released~~ published by ALICE Collaboration in ~~Ref.~~ [**?**].

The SC observables are defined as (for details see Sec. IV C in [**?**]):

$$\begin{aligned}\langle\langle\cos(m\varphi_1+n\varphi_2-m\varphi_3-n\varphi_4)\rangle\rangle_c &= \langle\langle\cos(m\varphi_1+n\varphi_2-m\varphi_3-n\varphi_4)\rangle\rangle \\ &\quad -\langle\langle\cos[m(\varphi_1-\varphi_2)]\rangle\rangle\langle\langle\cos[n(\varphi_1-\varphi_2)]\rangle\rangle \\ &= \langle v_m^2 v_n^2\rangle - \langle v_m^2\rangle\langle v_n^2\rangle\,, \end{aligned} \tag{3}$$

with the condition $m \neq n$ for two positive integers m and n. ~~The complete discussion can be found in Section IV C of Ref. [**?**].~~

In this article SC(m,n) ~~can be~~ normalized with the product $\langle v_m^2\rangle\langle v_n^2\rangle$~~to obtain *normalized* symmetric cumulants~~ [**?** **?**], ~~which we denote~~ is denoted by NSC(m,n)~~, i.e.~~ :

$$\mathrm{NSC}(m,n) \equiv \frac{\mathrm{SC}(m,n)}{\langle v_m^2\rangle\langle v_n^2\rangle}\,. \tag{4}$$

Normalized symmetric cumulants reflect only the degree of the correlation which is expected to be insensitive to the magnitudes of v_m and v_n, while SC(m,n) contains both the degree of the correlations between two different flow harmonics and individual v_n harmonics. In Eq. (4) the products in the denominator are obtained with two-particle correlations ~~and~~ using a pseudorapidity gap of $|\Delta\eta| > 1.0$ ~~to suppress~~ which suppresses biases from few-particle nonflow correlations. ~~On the other hand, in the~~ For the two two-particle correlations which appear in the definition of SC(m,n) in Eq. ~~3~~ (3) the pseudorapidity gap is not needed, since nonflow is suppressed by construction in ~~SC observable, as the study based on HIJING model has clearly demonstrated in Ref.~~ this case. This was verified by HIJING model simulations in [**?**].

The ~~first measurementsof SC observables~~ ALICE measurements [**?**] have revealed that fluctuations of v_2 and v_3 are anti-correlated, while fluctuations of v_2 and v_4 are correlated in all centralities [**?**]. However, the details of the centrality dependence differ in the fluctuation-dominated (most central) and the

geometry-dominated (mid-central) regimes [**?**]. ~~Most importantly, the~~ The observed centrality dependence of SC(4,2) cannot be captured with the constant η/s dependence, indicating clearly that the temperature dependence plays an important role~~in describing QGP's η/s dependence in various stages of heavy-ion evolution~~. These results were also used to discriminate between different parameterizations of initial conditions~~and it~~. It was demonstrated that in the fluctuation-dominated regime (~~in~~ central collisions) MC-Glauber initial conditions with binary collisions weights are favored over wounded nucleon weights [**?**].

~~The SC observables provide orthogonal information to recently measured symmetry plane correlators in Refs. [**? ? ?**]. This statement does not exclude the possibility that both set of observables can be sensitive to the same physical mechanisms. In the recent theoretical study [**?**] it was pointed out that the mechanism giving rise to symmetry plane correlations (nonlinear coupling) can also contribute to symmetric cumulants. As a concrete example it was discussed that the existing correlation due to hydrodynamic evolution between V_4 and V_2^2 (which are vectors in the transverse plane) implies that both the angles and the magnitudes are correlated [**?**].~~

~~Interpretation of flow results obtained with multiparticle correlation techniques in small colliding systems, like pp and p–Pb at LHC, remains a challenge. The underlying difficulty stems from the fact that when anisotropic flow harmonic v_n is estimated with k-particle correlator, the statistical spread of that estimate scales to leading order as $\sigma_{v_n} \sim \frac{1}{\sqrt{N}} \frac{1}{M^{k/2}} \frac{1}{v_n^{k-1}}$, where M is the number of particles in an event (multiplicity) and N is total number of events. This generic scaling ensures that multiparticle correlations are precision method only in heavy-ion collisions , characterized both with large values of multiplicity and flow. To leading order the measurements in small systems [**? ? ? ? ?**] and the measurements in heavy-ion collisions resemble the same features, which can be attributed to collective anisotropic flow in both cases. However, such interpretation is challenged by the outcome of recent Monte Carlo study [**?**] for e^+e^- systems in which collective effects are not expected. Nonetheless, in this study to leading order multiparticle correlations exhibit yet again the similar universal trends first seen in heavy-ion collisions, both for elliptic and triangular flow. Therefore, it seems unlikely that the analysis of individual flow harmonics with multiparticle techniques will answer whether collective effects can develop and QGP be formed in small systems—instead new observables, like SC, might provide the final answer due to their better sensitivity [**? ?**].~~

2.1 ~~Event and Track Selection~~

3 Data Analysis

~~The data sample~~ A sample of Pb–Pb collisions at $\sqrt{s_{\rm NN}} = 2.76$ TeV recorded by ALICE during the 2010 heavy-ion run at the LHC is used for this analysis. Detailed descriptions of the ALICE detector can be found in [**? ? ?**]. The Time Projection Chamber (TPC) was used to reconstruct charged particle tracks and measure their momenta with full azimuthal coverage in the pseudorapidity range $|\eta| < 0.8$. Two scintillator arrays (V0) which cover the pseudo-rapidity ranges $-3.7 < \eta < -1.7$ and $2.8 < \eta < 5.1$ were used for triggering and the determination of centrality [**?**]. The trigger conditions and the event selection criteria are identical to those described in [**? ?**]. Approximately 10^7 minimum-bias Pb–Pb events with a reconstructed primary vertex within ± 10 cm from the nominal interaction point in the beam direction are ~~used for this analysis~~selected. Charged particles reconstructed in the TPC in $|\eta| < 0.8$ and $0.2 < p_{\rm T} < 5$ GeV/c were selected. The charged track quality cuts described in [**?**] were applied to minimize contamination from secondary charged particles and fake tracks. The reconstruction efficiency and contamination of charged particles were estimated from HIJING Monte Carlo simulations [**?**] combined with a GEANT3 [**?**] detector model and were found to be independent of the collision centrality. The reconstruction efficiency increases from 70% to 80% for particles with $0.2 < p_{\rm T} < 1$ GeV/c and remains constant at (80 ± 5)% for $p_{\rm T} > 1$ GeV/c. The estimated contamination by secondary charged particles from weak decays and photon conversions is less than 6% at $p_{\rm T} = 0.2$ GeV/c and falls below

1% for $p_{\mathrm{T}} > 1$ GeV/c. ~~With this choice of low~~ The p_{T} cut-off ~~we are reducing~~ of 0.2 GeV/c reduces event-by-event biases ~~from smaller~~ due to small reconstruction efficiency at lower p_{T}, while the high p_{T} cut-off of 5 GeV/c ~~was introduced to reduce~~ reduces the contribution to the anisotropies from jets. Reconstructed TPC tracks were required to have at least 70 ~~TPC~~ space points (out of a maximum of 159). Only tracks with a transverse distance of closest approach (DCA) to the primary vertex less than 3 mm, both in longitudinal and transverse direction, are accepted~~to reduce~~. This reduces the contamination from secondary tracks ~~(for instance the charged particles~~ produced in the detector material, particles from weak decays, etc. ~~).~~ Tracks with kinks (the tracks that appear to change direction due to multiple scattering, $K^{\pm}$ decays) were rejected.

3.1 ~~Systematic Uncertainties~~

4 Systematic Uncertainties

The systematic uncertainties are estimated by varying the event and track selection criteria. All systematic checks described here are performed independently. All results of SC(m,n) with a selected criterion are compared to ones from the default event and track selection described in the previous section. The differences between the default results and the ones obtained from the variation of the selection criteria are taken as systematic uncertainty of each individual source. The contributions from different sources were ~~then~~ added in quadrature to obtain the ~~final value of the~~ total systematic uncertainty.

The event centrality was determined by the V0 detectors [**?**] with better than 2% resolution~~of centrality determination~~. The systematic uncertainty from centrality determination was evaluated by using TPC and Silicon Pixel Detector (SPD) [**?**] detectors instead of ~~the default,~~ V0 detectors. The systematic ~~uncertainties~~ uncertainty from the centrality determinations ~~were~~ is about 3% both for SC(5,2) and SC(4,3), and 8% for SC(5,3).

As described in Sec. 3, the reconstructed vertex position ~~in~~ along the beam axis (z-vertex) is required to be located within 10 cm of interaction point (IP) to ensure ~~an~~ a uniform detector acceptance for the tracks within $|\eta| < 0.8$ for all the vertices. The systematic uncertainty from z-vertex cut was estimated by reducing the z-vertex to 8cm and was found to be less than 3%.

The analyzed events were recorded with two settings of the ~~magnetic field polarities~~ L3 magnet polarity and the resulting data sets have almost the same number of events. Events with both ~~magnetic polarizations~~ magnet polarity were used for the default analysis and the systematic uncertainties were evaluated from ~~the results from~~ variation between each of two ~~polarized~~ magnetic field settings. Moreover, ~~because of incompleteness of track reconstruction, correction steps are necessary to trace back from reconstructed tracks to the originally generated particles from the collisions. The~~ the effects from p_{T} dependence reconstruction efficiency were taken into systematic uncertainty. Magnetic ~~polarizations~~ polarity variation and reconstruction efficiency effects are ~~relatively small and difference from the default settings were~~ less than 2%.

The systematic uncertainty due to the track reconstruction was estimated ~~using two additional tracking criteria, first relying on~~ from comparison between results for the so-called standalone TPC ~~tracking~~ tracks with the same parameters as described in Sec. 3, and ~~the second that relies on the~~ combination of the TPC and the Inner Tracking System (ITS) detectors with tighter selection criteria. To correct for non-uniform azimuthal acceptance due to dead zones in SPD, and to get the best transverse momentum resolution, approach of hybrid selection with SPD hit and/or ITS refit tracks combined with TPC were used. Then each track reconstruction was evaluated by varying the threshold on parameters used to select the tracks at the reconstruction level. The systematic difference of up to 12% was observed in SC(m,n) ~~results~~ from the different track selections. In addition, we applied the like-sign technique to estimate non-flow ~~effects on~~ contribution in SC(m,n). The difference between ~~both charged combinations and like-sign combinations were~~ results obtained by selecting all charged particles and results obtained after

either selecting only positively or only negatively charged particles was the largest contribution to the systematic uncertainty and ~~they were~~ it is about 7% for SC(4,3) and 20% for SC(5,3).

~~One of the other largest contributions~~ Another large contribution to the systematic uncertainty originates from the non-uniform reconstruction efficiency in azimuthal angle. In order to estimate ~~the effectson the measurements of these azimuthal correlators for various detector inefficiencies~~its effects, we use the AMPT ~~models (see the details in~~ model (see Sec. 6) which have flat uniform distribution of azimuthal angles. ~~Then we enforce detector inefficiencies by imposing~~ Detector inefficiencies was introduced to mimic non-uniform azimuthal distribution ~~from~~ in the data. For the observables ~~,~~ SC(5,2), SC(5,3) and SC(4,3) ~~, the uncertainties from the~~ variation due to non-uniform ~~distribution of azimuthal angles were~~ acceptance is about 9%, 17% and 11%, respectively. ~~Generally,~~ Overall, the systematic uncertainties are larger for the SC(5,3) and SC(5,2) than for the lower harmonics of SC(m,n)~~, because smaller values of v_n are~~ . This is because v_n are decreasing with n increasing and become more sensitive to azimuthal modulation ~~and v_n decreases with n increasing.~~

5 ~~Theoretical models~~

~~We have used various models in this article. The HIJINGmodel [? ?] was utilized to obtain the p_{T}-weights [?] which were used to estimate systematic bias due to non-uniform reconstruction efficiency as a function of transverse momentum~~due to detector imperfections.

~~We have compared the centrality dependence of our observables with theoretical model from [?], where the initial energy density profiles are calculated using a next-to-leading order perturbative-QCD+saturation model [? ?]. The subsequent spacetime evolution is described by relativistic dissipative fluid dynamics with different parameterizations for the temperature dependence of the shear viscosity to entropy density ratio $\eta/s(T)$. Each of the $\eta/s(T)$ parameterizations is adjusted to reproduce the measured v_n from central to mid-peripheral collisions.~~

~~The VISH2+1 [? ?] is an event-by-event theoretical model for relativistic heavy-ion collisions based on (2+1)-dimensional viscous hydrodynamics which describes both the QGP phase and the highly dissipative and even off-equilibrium late hadronic stage with fluid dynamics. With well tuned transport coefficients, decoupling temperature and some initial conditions (like AMPT [? ? ?] etc.), it could fit many related soft hadron data, such as the p_{T} spectra and different flow harmonics at RHIC and the LHC [? ? ? ?]. Three different initial conditions (MC-Glauber, MC-KLNand AMPT) along with different constant η/s values are used in the model [?]. Traditionally, the Glauber model constructs the initial entropy density of the QGP fireball from a mixture of the wounded nucleon and binary collision density profiles [?], and the KLNmodel assumes that the initial entropy density is proportional to the initial gluon density calculated from the corresponding k_T factorization formula [?]. In the Monte Carlo versions (MC-Glauberand MC-KLN) [? ? ?], additional initial state fluctuations are introduced through the position fluctuations of individual nucleons inside the colliding nuclei. For the AMPTinitial conditions [? ? ?], the fluctuating energy density profiles are constructed from the energy decompositions of individual partons, which fluctuate in both momentum and position coordinate. Compared with the MC-Glauberand MC-KLNinitial conditions, the additional Gaussian smearing parameter in the AMPTinitial conditions makes the typical initial fluctuation scales changeable which gives rise to non-vanishing initial local flow velocities [?].~~

~~Finally, we provide an independent estimate of the centrality dependence of our observables by utilizing the AMPTmodel [? ? ?]. Even though thermalization could be achieved in collisions of very large nuclei and/or at extremely high energy, the dense matter created in heavy-ion collisions may not reach full thermal or chemical equilibrium as a result of its finite volume and energy. To address such non-equilibrium many-body dynamics, AMPT has been developed, which includes both initial partonic and final hadronic interactions and the transition between these two phases of matter. For the initial conditions, the AMPT model uses the spatial and momentum distributions of hard minijet partons and soft strings from the~~

~~HIJING model [? ?]. The AMPT model can be run in two main configurations, the default and the string melting model. In the default version, partons are recombined with their parent strings when they stop interacting. The resulting strings are later converted into hadrons using the Lund string fragmentation model [? ?]. In the string melting version, the initial strings are melted into partons whose interactions are described by the ZPC parton cascade model [?]. These partons are then combined into the final state hadrons via a quark coalescence model. In both configurations, the dynamics of the subsequent hadronic matter is described by a hadronic cascade based on A Relativistic Transport (ART) model [?] which also includes resonance decays. The third version presented in this article is based on the string melting configuration, in which the hadronic rescattering phase is switched off to study its influence to the development of anisotropic flow. The input parameters used in both configurations are: $\alpha_s = 0.33$, a partonic cross-section of 1.5 mb, while the Lund string fragmentation parameters were set to $a = 0.5$ and $b = 0.9$ GeV^{-2}. Even though the string melting version of AMPT [? ?] reasonably reproduces particle yields, p_{T} spectra, and v_2 of low-p_{T} pions and kaons in central and mid-central Au–Au collisions at $\sqrt{s_{\mathrm{NN}}} = 200$ GeV and Pb–Pb collisions at $\sqrt{s_{\mathrm{NN}}} = 2760$ GeV [?], it was seen clearly in the recent study [?] that it fails to quantitatively reproduce the harmonic flow coefficients of identified hadrons (v_2, v_3, v_4 and v_5) at $\sqrt{s_{\mathrm{NN}}} = 2760$ GeV. It turns out that the radial flow in AMPT is 25% lower than the measured value at the LHC, which indicates that the unrealistically low radial flow in AMPT is responsible for the quantitative disagreement [?]. The details of configurations of AMPT settings used for this article and the comparisons of p_{T} differential v_n for pions, kaons and protons to the data can be found in [?].~~

5 Results

The centrality dependence of the higher order harmonic correlations (SC(4,3), SC(5,2) and SC(5,3)) are presented in Fig. 1 and compared to the lower order harmonic correlations (SC(4,2) and SC(3,2)) which are taken from ~~the recent publication~~ [?]. The correlation between v_3 and v_4 is negative, and similarly for v_3 and v_2, while the other correlations are all positive, which reveals that v_2 and v_5, v_3 and v_5 are correlated as v_2 and v_4, while v_3 and v_4 are anti-correlated as v_3 and v_2.

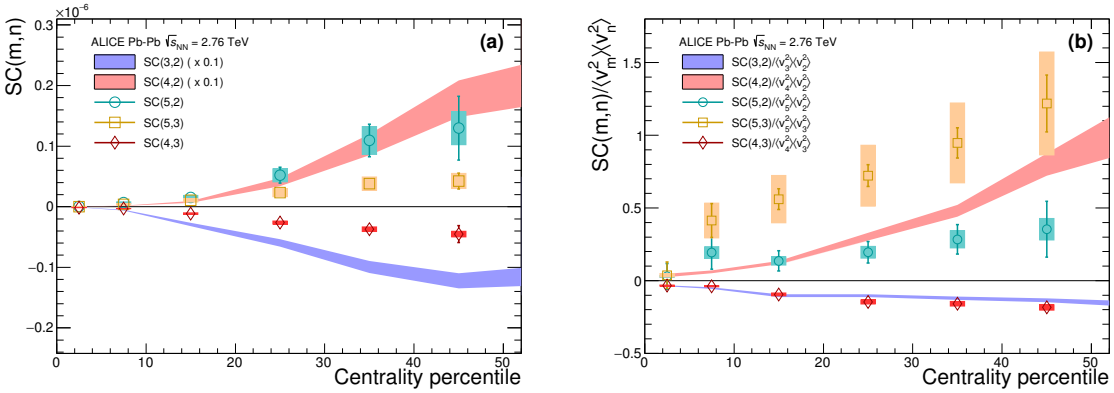

Fig. 1: ~~The result of~~ SC(m,n) (~~left figure~~a) and NSC(m,n) (~~right figure~~b) with flow harmonic ~~order~~ up to 5$^{\mathrm{th}}$ order in Pb–Pb collisions at $\sqrt{s_{\mathrm{NN}}} = 2.76$ TeV. The lower order harmonic correlations (SC(3,2), SC(4,2), NSC(3,2) and NSC(4,2)) are taken from ~~the recent publication~~ [?] and shown as bands. Note that the systematic and statistical errors are combined quadratically for these lower order harmonic correlations and SC(4,2) and SC(3,2) on the ~~left figure~~ panel (a) are scaled ~~down~~ by factor of ~~10.~~0.1.

The higher order flow harmonic correlations (SC(4,3), SC(5,2) and SC(5,3)) are much smaller compared to the lower order harmonic correlations (SC(3,2) and SC(4,2)). In particular SC(5,2) is 10 times smaller than SC(4,2) and SC(4,3) is about 20 times smaller that SC(3,2).

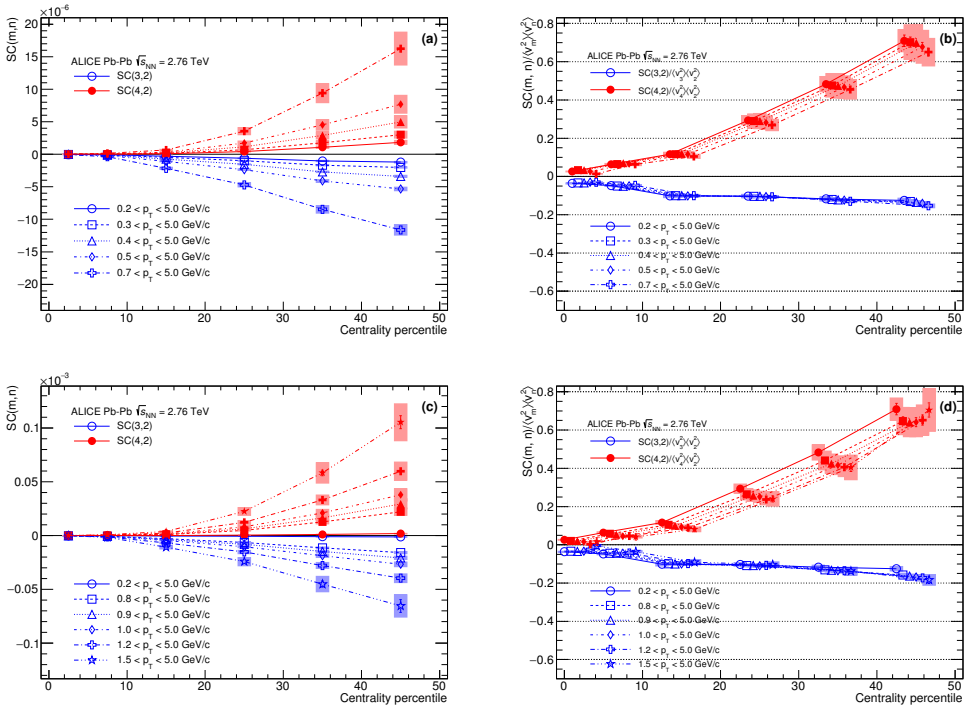

Fig. 2: SC(3,2) and SC(4,2) with various minimum p_{T} cuts ((a) and (c)) and results of normalized SC(3,2) and SC(4,2) ((b) and (d)) in Pb–Pb collisions at $\sqrt{s_{\mathrm{NN}}} = 2.76$ TeV. The panel (a) and (b) show the results for minimum p_{T} range, $0.2 < p_{\mathrm{T}} < 0.7$ GeV/c and the panel (c) and (d) are for minimum p_{T} range, $0.8 < p_{\mathrm{T}} < 1.5$ GeV/c. Note that NSC data points from each minimum p_{T} in a centrality percentile bin are shifted for visibility.

However, unlike SC(m,n), the NSC(m,n) results with the higher order flow harmonics show almost the same order of the correlation strength as the lower order flow harmonic correlations (NSC(3,2) or NSC(4,2)). NSC(4,3) magnitude is comparable to NSC(3,2) and one finds that a hierarchy, NSC(5,3) $>$ NSC(4,2) $>$ NSC(5,2), holds for centrality ranges $> 20\%$ within the errors shown on the ~~right~~ panel (b) in Fig. 1. These results indicate that the lower order harmonic correlations (SC(3,2) and SC(4,2)) are larger than higher order harmonic correlations (SC(4,3), SC(5,2) and SC(5,3)), not only because of the correlation strength itself but also because of the strength of individual flow harmonics. SC(5,2) is stronger than SC(5,3), but as for NSC, the normalized correlation between v_5 and v_3 is stronger than the normalized correlation between v_5 and v_2.

It can be seen on the panel (a) in Fig. 1 that the lower order harmonic correlations (SC(3,2) and SC(4,2)) and SC(5,2) increase non-linearly toward peripheral collisions. In case of SC(5,3) and SC(4,3), the centrality dependence is weaker than the other harmonic correlations and a monotonic increase is observed for these harmonic correlations. NSC(5,3) shows the strongest ~~centrality dependence among all harmonic correlations~~ correlation among all harmonics and NSC(4,2), NSC(5,2) shows a weak centrality dependence. Both NSC(3,2) and NSC(4,3) show a monotonic increase toward peripheral collisions with the similar magnitude.

~~To obtain~~

To study the p_{T} dependence of SC(m,n)~~results, we vary minimum~~ , we change the low p_{T} ~~cuts~~cut-off, instead of using independent p_{T} ~~bin-by-bin~~ interval, in order to avoid large statistical fluctuations in the results. Various minimum p_{T} cuts from 0.2 to 1.5 GeV/c are applied. The results of p_{T} dependence of SC(3,2) and SC(4,2) with minimum p_{T} cuts, $0.2 < p_{\mathrm{T}} < 0.7$ GeV/c, are shown on the ~~left top~~ panel (a) in Fig. 2. The strength of SC(m,n) becomes larger as the minimum p_{T} increases. This p_{T} dependent

correlations have much stronger centrality dependence, where SC(m,n) gets much larger as the centrality or the minimum p_{T} cut increase. NSC(3,2) and NSC(4,2) with different minimum cuts are shown on the ~~right~~ panel (b) and (d) in Fig. 2. The strong p_{T} dependence observed in SC(m,n) is not ~~clearly~~ seen in NSC(m,n). The NSC(m,n) results are aligned all together and consistent in errors for all minimum p_{T} cuts. This ~~may indicate~~ indicates that the p_{T} dependence of SC(m,n) ~~does not solely result from the correlation between flow harmonics but results from the~~ is dominated by the p_{T} ~~dependent individual v_n~~ dependence of $\langle v_n \rangle$ values. The minimum p_{T} cuts are extended from 0.8 to 1.5 GeV/c and the results are shown on the ~~bottom panels~~ panel (c) and (d) in Fig. 2. ~~As for~~ While SC(m,n) ~~,~~ show the similar trends ~~are observed~~ as for $p_{\mathrm{T}} < 0.8$ GeV/c, ~~however~~ NSC(m,n) tends to decrease ~~as the minimum~~ with increasing p_{T} or the centrality~~increase~~. The p_{T} dependence for NSC(3,2) is not clearly seen and it is consistent with no p_{T} dependence within the current statistical and systematic errors for the centrality range <30% and shows moderate decreasing trend for increasing p_{T} for >30% centrality range. NSC(4,2) shows a moderate decreasing trend as p_{T} or the centrality increase. These observations are strikingly different from p_{T} dependence of individual flow harmonics, where the relative flow fluctuations $\sigma_{v_2}/\langle v_2 \rangle$ [**?**] are independent of momentum up to $p_{\mathrm{T}} \sim 8$ GeV/c (see Fig. 3 in Ref. [**?**]).

~~SC(3,2) and SC(4,2) with various minimum p_{T} cuts (left) and results of normalized SC(3,2) and SC(4,2) (right). The upper panels show the results for minimum p_{T} range, $0.2 < p_{\mathrm{T}} < 0.7$ GeV/c and the bottom panels are for minimum p_{T} range, $0.8 < p_{\mathrm{T}} < 1.5$ GeV/c. Note that NSC data points from each minimum p_{T} in a centrality percentile bin are shifted for visibility.~~

6 Model Comparisons

We have compared the centrality dependence of our observables with the event-by-event EKRT+viscous hydrodynamic calculations [**?**], where the initial energy density profiles are calculated using a next-to-leading order perturbative-QCD+saturation model [**? ?**]. The subsequent spacetime evolution is described by relativistic dissipative fluid dynamics with different parameterizations for the temperature dependence of the shear viscosity to entropy density ratio $\eta/s(T)$. This model gives a good description of the charged hadron multiplicity and the low p_{T} region of the charged hadron spectra at RHIC and the LHC (see Fig. 11-13 in [**?**]). Each of the $\eta/s(T)$ parameterizations is adjusted to reproduce the measured v_n from central to mid-peripheral collisions (see Fig. 14 in [**?**]).

The VISH2+1 [**? ?**] event-by-event calculations for relativistic heavy-ion collisions are based on (2+1)-dimensional viscous hydrodynamics which describes both the QGP phase and the highly dissipative and even off-equilibrium late hadronic stage with fluid dynamics. With well tuned transport coefficients, decoupling temperature and given initial condition discussed later, it could describe the p_{T} spectra and different flow harmonics at RHIC and the LHC [**? ? ? ?**]. Three different initial conditions (MC-Glauber, MC-KLN and AMPT) along with different constant η/s values are used in the model [**?**]. Traditionally, the Glauber model constructs the initial entropy density from contributions of the wounded nucleon and binary collision density profiles [**?**], and the KLN model assumes that the initial entropy density is proportional to the initial gluon density calculated from the corresponding k_T factorization formula [**?**]. In the Monte Carlo versions (MC-Glauber and MC-KLN) [**? ? ?**], additional initial state fluctuations are introduced through the position fluctuation of individual nucleons inside the colliding nuclei. For the AMPT initial conditions [**? ? ?**], the fluctuating energy density profiles are constructed from the energy decompositions of individual partons, which fluctuate in both momentum and position coordinate. Compared with the MC-Glauber and MC-KLN initial conditions, the additional Gaussian smearing in the AMPT initial conditions gives rise to non-vanishing initial local flow velocities [**?**].

The centrality dependence of SC observables is compared to that in the AMPT model [**? ? ?**]. Even though thermalization could be achieved in collisions of very large nuclei and/or at extremely high energy [**?**], the dense matter created in heavy-ion collisions may not reach full thermal or chemical

equilibrium as a result of its finite volume and short time scale. To address such non-equilibrium many-body dynamics, AMPT has been developed, which includes both initial partonic and final hadronic interactions and the transition between these two phases of matter. For the initial conditions, the AMPT model uses the spatial and momentum distributions of hard minijet partons and soft strings from the HIJING model [**?** **?**]. The AMPT model can be run in two main configurations, the default and the string melting model [1]. In the default version, partons are recombined with their parent strings when they stop interacting. The resulting strings are later converted into hadrons using the Lund string fragmentation model [**?** **?**]. In the string melting version, the initial strings are melted into partons whose interactions are described by the ZPC parton cascade model [**?**]. These partons are then combined into the final state hadrons via a quark coalescence model. In both configurations, the dynamics of the subsequent hadronic matter is described by a hadronic cascade based on A Relativistic Transport (ART) model [**?**] which also includes resonance decays. The third version used in this article is based on the string melting configuration, in which the hadronic rescattering phase is switched off to study its influence to the development of anisotropic flow. Even though the string melting version of AMPT [**?** **?**] reasonably reproduces particle yields, p_{T} spectra, and v_2 of low-p_{T} pions and kaons in central and mid-central Au–Au collisions at $\sqrt{s_{\mathrm{NN}}} = 200$ GeV and Pb–Pb collisions at $\sqrt{s_{\mathrm{NN}}} = 2.76$ TeV [**?**], it was seen clearly in the recent study [**?**] that it fails to quantitatively reproduce the harmonic flow coefficients of identified hadrons (v_2, v_3, v_4 and v_5) at $\sqrt{s_{\mathrm{NN}}} = 2.76$ TeV. It turns out that the radial flow in AMPT is 25% lower than the measured value at the LHC, which indicates that the unrealistically low radial flow in AMPT is responsible for the quantitative disagreement [**?**]. The details of configurations of AMPT settings used for this article and the comparisons of p_{T} differential v_n for pions, kaons and protons to the data can be found in [**?**].

6.1 Low Order Harmonic Correlations

SC(3,2) and SC(4,2) are compared to several theoretical calculations. ~~First, the~~ The event-by-event EKRT+viscous hydrodynamic predictions with the different parameterizations for the temperature dependence of the shear viscosity to entropy density ratio $\eta/s(T)$ are shown ~~on the~~ in Fig. 2 ~~in~~ of Ref. [**?**]. It has been demonstrated that NSC(3,2) observable is sensitive mainly to the initial conditions, while NSC(4,2) observable is sensitive to both the initial conditions and the system properties, which is consistent with the predictions from [**?**]. However, the sign of NSC(3,2) is positive in the models in 0-10% central collisions while it is negative in data. In the most central collisions the anisotropies originate mainly from fluctuations, i.e. the initial ellipsoidal geometry characteristic for mid-central collisions plays little role in this regime. ~~Hence this observation will help to understand~~ This observation helps to understand better the fluctuations in initial ~~conditions better~~energy density. NSC(4,2) observable shows better sensitivity for different $\eta/s(T)$ parameterizations but the model cannot describe neither the centrality dependence nor the absolute values. ~~These~~ This observed distinct discrepancy between data and theoretical predictions ~~indicate~~ indicates that the current understanding of initial conditions used to model the initial stages of heavy-ion collision need to be revisited to further constrain the $\eta/s(T)$, considering the difficulties ~~on~~ in separating the role of the η/s from the initial conditions to the final state particle anisotropies [**?** **?**]. ~~Hence the~~ The use of SC(m,n) and NSC(m,n) can provide new constraints on the detailed modeling of ~~the initial state conditionsand the fluctuations of the medium created in heavy-ion collisions~~fluctuating initial conditions. The better constraints on the initial state conditions will certainly reduce the uncertainties of determining $\eta/s(T)$.

~~Results of SC(3,2) and SC(4,2) are compared to various VISH2+1 calculations [**?**] with different settings. Three initial conditions from AMPT, MC-KLN, and MC-Glauber are drawn as different colors and markers. The η/s parameters are shown as different line styles, the small shear viscosities ($\eta/s = 0.08$) are shown as solid lines, and large shear viscosities ($\eta/s = 0.2$ for MC-KLN and MC-Glauber, 0.16 for~~

[1] The input parameters used in both configurations are: $\alpha_s = 0.33$, a partonic cross-section of 1.5 mb, while the Lund string fragmentation parameters were set to $\alpha = 0.5$ and $b = 0.9$ GeV^{-2}.

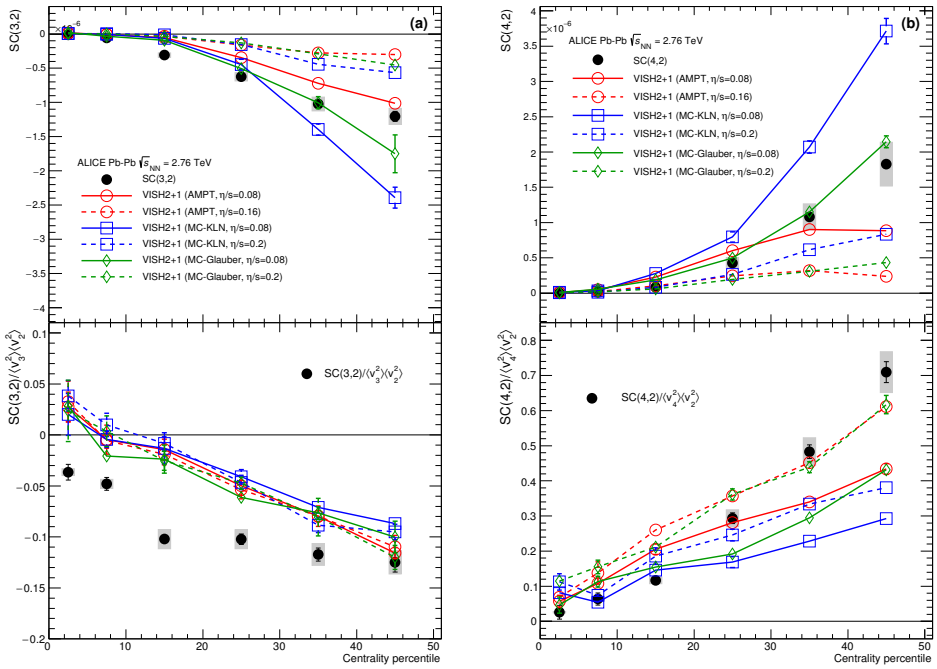

Fig. 3: ~~Results of~~ SC(3,2) (a) and SC(4,2) (b) in Pb–Pb collisions at $\sqrt{s_{\rm NN}} = 2.76$ TeV are compared to various ~~AMPT models~~VISH2+1 calculations [**?**] with different settings. Upper (lower) panels ~~are the results of~~ show SC~~(m,n)~~ (m,n) (NSC(m,n)). Calculations with three initial conditions from AMPT, MC-KLN, and ~~the lower panels~~ MC-Glauber are ~~the results of NSC(m,n)~~drawn as different colors and markers. The ~~details of~~ η/s parameters are shown in line styles, the small $\eta/s = 0.08$ are shown as solid lines, and large $\eta/s = 0.2$ for MC-KLN and MC-Glauber, 0.16 for AMPT ~~configurations can be found in Sec~~are drawn as dashed lines. ~~??.~~

~~AMPT) are drawn as dashed lines. Upper panels are the result of SC(m,n) and lower panels are the results of NSC(m,n).~~

The results with the comparison to VISH2+1 calculation [**?**] are shown in Fig. 3. All ~~the models~~ calculations with large η/s regardless of the initial conditions ($\eta/s = 0.2$ for MC-KLN and MC-Glauber initial conditions and $\eta/s = 0.16$ for AMPT initial condition) fail to capture the centrality dependence of SC(3,2) and SC(4,2). ~~On the other hand, among the models~~ Among the calculations with small η/s ($\eta/s = 0.08$), the one with the AMPT initial condition describes the data better both for SC(3,2) and SC(4,2) in general but it cannot describe the data quantitively for most of the centrality ranges. Similarly ~~as the above mentioned~~ to the event-by-event EKRT+viscous hydrodynamic calculations [**?**], the sign of the normalized NSC(3,2) in ~~these models~~ the model calculations in Fig 3 is opposite to ~~its signature in the~~ that in data in 0-10% central collisions. NSC(3,2) does not show sensitivity to the initial conditions nor to the different η/s parameterizations used in the models and cannot be described by these models quantitively. However NSC(4,2) is sensitive both to the initial conditions and the η/s parameterizations used in the models. Even though NSC(4,2) favors both AMPT initial condition with $\eta/s = 0.08$ and MC-Glauber initial condition with $\eta/s = 0.20$, SC(4,2) can be only described by smaller η/s from AMPT and MC-Glauber initial conditions. Hence the ~~MC-Glauber initial condition with~~ calculations with large $\eta/s = 0.20$ ~~can be~~ is ruled out. We ~~come to a conclusion based on the tested model parameters~~ conclude that η/s should be small and AMPT initial condition is favored by the data.

~~Finally,the extracted results for final state particles~~ The SC(m,n) calculated from AMPT simulations ~~in the same way as for the data are compared~~ are compared to data in Fig. 4. As for SC(3,2), none of the ~~settings~~ calculations can describe the data and the ~~setting~~ calculation with the default AMPT

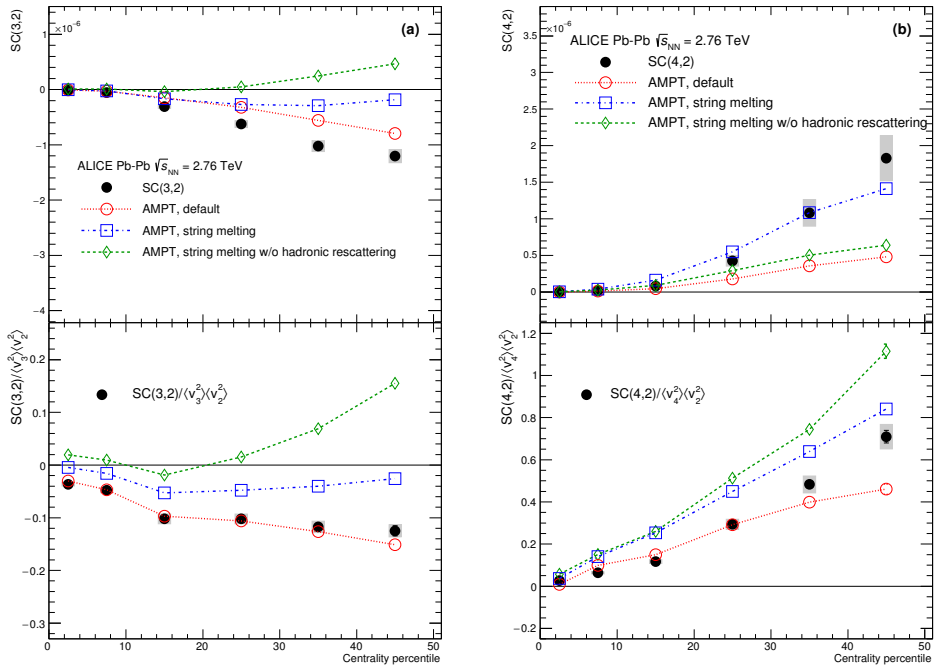

Fig. 4: SC(3,2) (a) and SC(4,2) (b) in Pb–Pb collisions at $\sqrt{s_{\rm NN}} = 2.76$ TeV are compared to various AMPT models. Upper panels (lower) are the results of SC(m,n) (NSC(m,n)).

model somewhat setting follows the trend of the data closest. The same setting can describe NSC(3,2) fairly well and also the sign default calculation can describe the sign and magnitude of NSC(3,2) is well reproduced by this setting while all while the hydrodynamic calculations in this article failed to describe the sign and magnitude of the observable in the most central collisions. Interestingly the string melting AMPT model cannot capture the data well where reproduce the data and the strength of the correlation is weaker than the default modelin data. The third version based on the string melting configuration with without the hadronic rescattering phase off is also shownto quantify its influence. This late . The hadronic rescattering stage makes both SC(3,2) and NSC(3,2) stronger in the string melting AMPT model but it is not enough to describe the data. Further we investigated why the default AMPT model can describe NSC(3,2) fairly well but underestimates SC(3,2). By taking the differences in the individual flow harmonics (v_2 and v_3) between the model and data into account, we were able to recover the difference in SC(3,2) between the data and the model. The discrepancy in SC(3,2) can be explained by the overestimated individual v_n values reported in [**?**] in all the centrality ranges.

In the case of SC(4,2), the string melting AMPT model can fairly well describe the data while the default model underestimates it. NSC(4,2) is slightly overestimated by the same setting which can describe SC(4,2) but the default AMPT model can describe the data better. The influence of the hadronic rescattering phase for NSC(4,2) is opposite to other observables (SC(3,2), NSC(3,2) and SC(4,2)), where the . The hadronic rescattering makes NSC(4,2) slightly smaller. It should be noted that the better agreement for SC(m,n) should not be overemphasized since there are discrepancies in the individual v_n between the AMPT models and the data as it was demonstrated for SC(3,2). Hence the simultaneous description of SC(m,n) and NSC(m,n) should give better constraints to the parameters in AMPT models.

6.2 Higher Order Harmonic Correlations

The higher order harmonic correlations (SC(4,3), SC(5,2) and SC(5,3)) are compared to several theoretical calculations. First, the The event-by-event EKRT+viscous hydrodynamic predictions with the

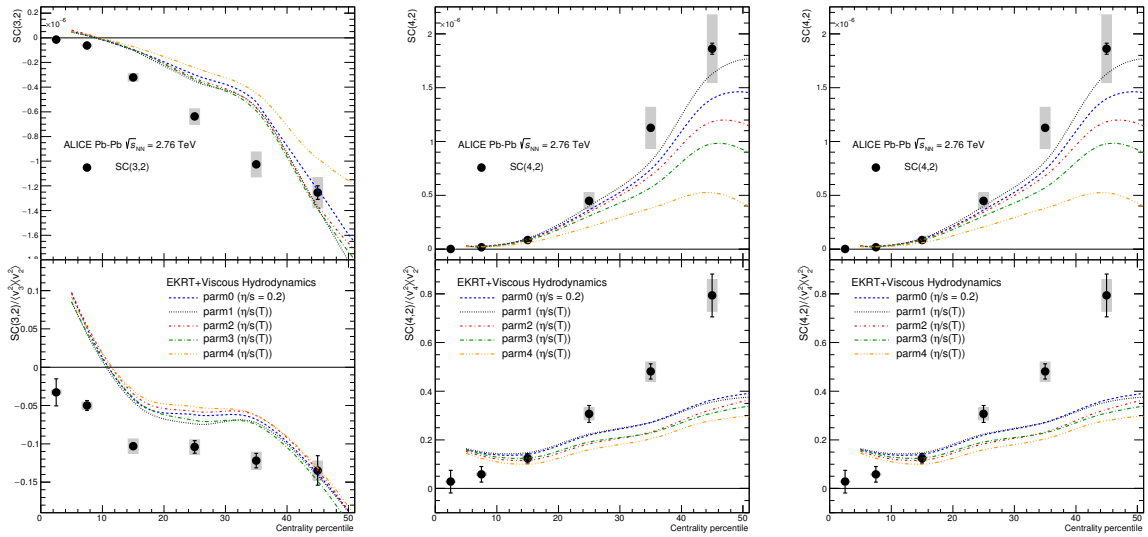

Fig. 5: Results ~~from~~ of SC(~~*m*~~5,~~*n*~~2), SC(5,3) and SC(4,3) in Pb–Pb collisions at $\sqrt{s_{\rm NN}} = 2.76$ TeV are compared to the event-by-event EKRT+viscous hydrodynamic calculations [**?**]. The dashed lines are hydrodynamic predictions with various $\eta/s(T)$ parameterizations [**?**]. ~~This~~ These SC(3,2) and SC(4,2) will be replaced with new figures for higher order correlations once we have the calculations from Harri Niemi et. al [**?**].

different parameterizations for the temperature dependence of the shear viscosity to entropy density ratio $\eta/s(T)$ are shown ~~on the left~~ in Fig. 5. **[Waiting for $\eta/s(T)$ hydro calculations from Harri Niemi et. al [?], figure will be replaced later, just a place holder]**

The higher order harmonic correlations (SC(4,3), SC(5,2) and SC(5,3)) are compared to VISH2+1 calculations [**?**], shown in Fig. 6. All the models with large η/s regardless of the initial conditions ($\eta/s = 0.2$ for MC-KLN and MC-Glauber initial conditions, and $\eta/s = 0.16$ for AMPT) failed to capture the centrality dependence of SC(5,2), SC(5,2) and SC(5,3), more clearly than for the lower order harmonic correlations (SC(3,2) and SC(4,2)). Among the models with small η/s ($\eta/s = 0.08$), the one from the AMPT initial condition describes the data much better than the ones with other initial conditions. A quite clear separation between different initial conditions is observed for these higher order harmonic correlations compared to the lower order harmonic correlations. NSC(5,2) and SC(5,3) are quite sensitive to both the initial conditions and the η/s parameterizations. Similarly as the above mentioned hydrodynamic calculations [**?**], the sign of the NSC(4,3) in these models is opposite to its signature in the data in 0-10% central collisions. NSC(4,3) shows sensitivity to both initial conditions and η/s parameterizations. SC(4,3) data is clearly favored by smaller η/s but NSC(4,3) cannot be described by these models quantitively.

The extracted results for final state particles from AMPT simulations in the same way as for the data are compared in Fig. 7. The string melting AMPT model describes SC(5,3) and NSC(5,3) well. The same setting overestimates SC(5,2) and NSC(5,2). However the default AMPT model can describe NSC(5,3) and NSC(5,2) fairly well as it is the case for NSC(3,2) and NSC(4,2) seen in Fig. 4. In the case of SC(4,3), neither of the settings can describe the data but the default AMPT model follows the data closest. The string melting AMPT model fails to describe SC(4,3) and NSC(4,3). In summary, the default AMPT model describes well the normalized symmetric cumulants (NSC(m,n)) from lower to higher order harmonic correlations while the string melting AMPT model overestimates NSC(5,2) and underestimates (or predicts very weak correlation) NSC(4,3).

As discussed in Sec. 5, a hierarchy NSC(5,3) $>$ NSC(4,2) $>$ NSC(5,2) holds for centrality ranges $> 20\%$

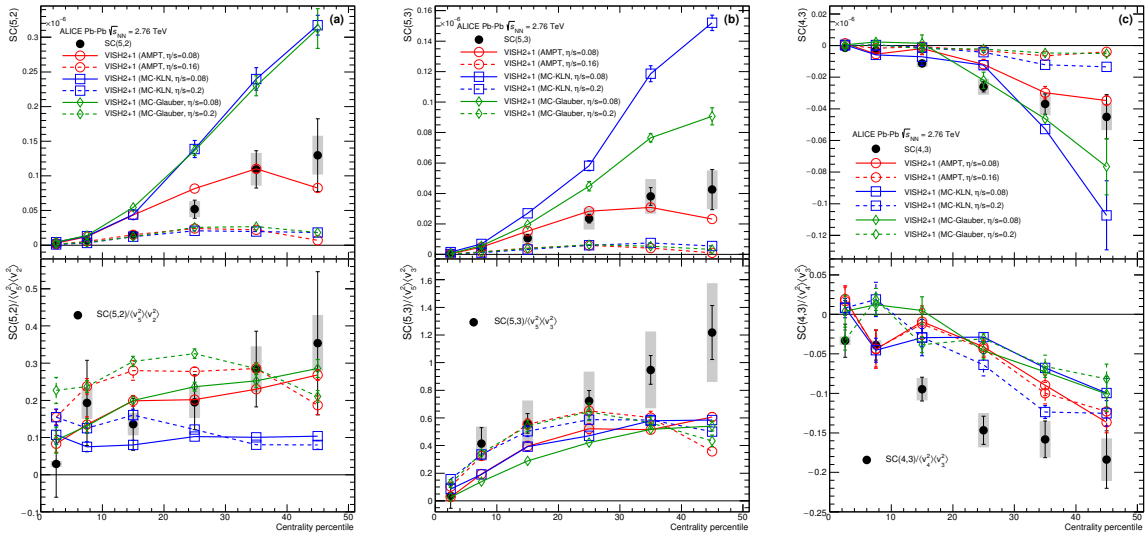

Fig. 6: Results of SC(5,2), SC(5,3) and SC(4,3) in Pb–Pb collisions at $\sqrt{s_{\rm NN}} = 2.76$ TeV are compared to various VISH2+1 calculations [**?**]. Three initial conditions from AMPT, MC-KLN and MC-Glauber are drawn as different colors and markers. The η/s parameters are shown as different line styles, the small shear viscosity ($\eta/s = 0.08$) are shown as solid lines, and large shear viscosities ($\eta/s = 0.2$ for MC-KLN and MC-Glauber, 0.16 for AMPT) are drawn as dashed lines. Upper panels are the results of SC(m,n) and lower panels are the results of NSC(m,n).

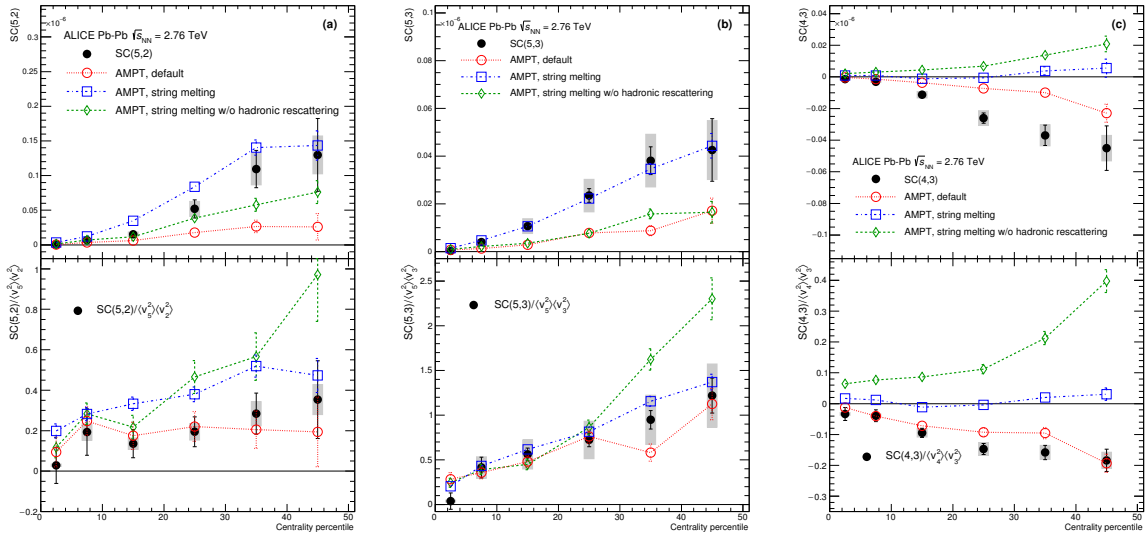

Fig. 7: Results of SC(5,2), SC(5,3) and SC(4,3) in Pb–Pb collisions at $\sqrt{s_{\rm NN}} = 2.76$ TeV are compared to various AMPT models. Upper panels are the results of SC(m,n) and the lower panels are the results of NSC(m,n). ~~The details of the AMPT configurations can be found in Sec. **??**.~~

within the errors and NSC(5,2) is smaller than NSC(5,3) while SC(5,2) is larger that SC(5,3). Except for 0-10% centrality range, we found that the same hierarchy also holds for the hydrodynamic calculations and the AMPT models in this article. The observed difference between SC(5,2) and SC(5,3) (SC(5,2) $>$ SC(5,3)) can be explained by the difference of the individual flow harmonics ($v_2 > v_3$). The opposite trend are observed for the normalized SC (NSC(5,3) $>$ NSC(5,2)). This can be attributed to the fact that the flow fluctuation is stronger for v_3 than v_2 [**?**]. It was claimed in Ref. [**?**] and seen also in Ref. [**?**] based on a AMPT model. NSC(m,n) correlators increase with the larger η/s in hydrodynamic calculations in 0-30% centrality range in the same way as the event plane correlations [**? ?**]. In semi-peripheral collisions (>40%), the opposite trend is observed.

We list here important findings from the model comparison:

(i) NSC(3,2) observable is sensitive mainly to the initial conditions, while NSC(4,2) observable is sensitive to both the initial conditions and the temperature dependence of η/s.

(ii) All the VISH2+1 model calculations with large η/s regardless of the initial conditions failed to capture the centrality dependence of correlations.

(iii) Among the VISH2+1 model calculations with small η/s ($\eta/s = 0.08$), the one with the AMPT initial condition describes the data better in general but it cannot describe the data quantitively for most of the centrality ranges.

(iv) The correlation strength of v_3 and v_2, v_4 and v_3 (NSC(3,2) and NSC(4,3)) is underestimated in hydrodynamic model calculations.

(v) The sign of NSC(3,2) in 0-10% central collisions was found to be different between the data and hydrodynamic model calculations while the default AMPT model can reproduce the sign.

(vi) The default AMPT model can describe the normalized symmetric cumulants (NSC(m,n)) quantitively for most of centralities while the string melting AMPT model fails to describe them.

(vii) A hierarchy NSC(5,3) $>$ NSC(4,2) $>$ NSC(5,2) holds for centrality ranges $>$ 20% within the errors. This hierarchy is well reproduced both by hydrodynamic and AMPT model calculations.

6.3 Transverse Momentum Dependence of ~~Low Order Harmonic~~ Correlations between v_2, v_3 and v_4

It can be seen in Fig. 2 that the p_{T} dependence for NSC(3,2) is not clearly seen and it is consistent with no p_{T} dependence for the centrality range <30% and shows moderate decreasing trend for increasing p_{T} for >30% centrality range. NSC(4,2) shows a moderate decreasing trend as p_{T} or the centrality increase. In oder to see the trend more clearly, we show NSC(m,n) results as a function of minimum p_{T} cut in Fig. 8.

NSC(3,2) and NSC(4,2) as a function of different minimum p_{T} cut are compared to the AMPT simulations in Fig. 8. These observed p_{T} dependence for NSC(3,2) and NSC(4,2) in mid-central collisions is seen also in AMPT simulations for higher minimum p_{T} cuts. The other AMPT configurations except for the default AMPT model give very strong p_{T} dependence above 1 GeV/c and cannot describe the magnitude of the data both for NSC(3,2) and NSC(4,2) simultaneously. In the case of NSC(3,2), the default AMPT model describes the magnitude and p_{T} dependence well in all collision centralities except for $40-50\%$ where the model underestimates the data and have stronger p_{T} dependence than the data. As for NSC(4,2), the same model which describes NSC(3,2) also can reproduce the data well expect for $10-20\%$ and $40-50\%$ centralities where some deviations from the data both for the magnitude and p_{T} dependence are observed. When the string melting AMPT model is compared to the same model with the hadronic rescattering off, it is observed that the very

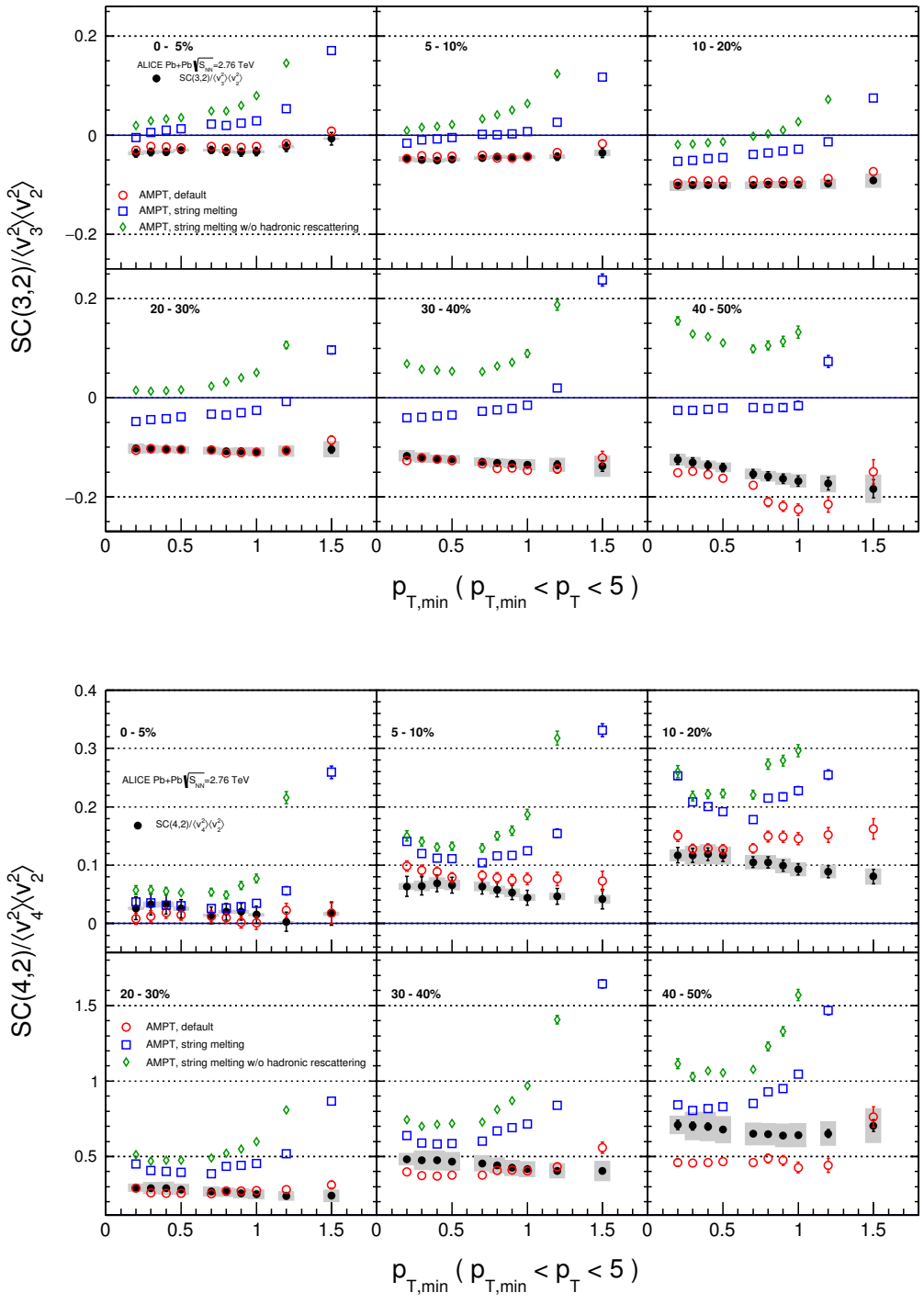

Fig. 8: NSC(3,2) (Top) and NSC(4,2) (Bottom) as a function of minimum p_{T} cuts in Pb–Pb collisions at $\sqrt{s_{\mathrm{NN}}} = 2.76$ TeV are compared to various AMPT models. ~~The details of the AMPT configurations can be found in Sec. ??.~~

strong p_{T} dependence as well as the correlation strength get weaker by the hadronic rescattering. This might imply that the hadronic interaction is the source of this observed p_{T} dependence even though the relative contributions from partonic and hadronic stage in the final state particle should be studied further. This observed moderate p_{T} dependence in mid-central collisions both for NSC(3,2) and NSC(4,2) might be an indication of possible viscous corrections for the equilibrium distribution at hadronic freeze-out predicted in [**?**]. The comparisons to hydrodynamic models can further help to understand the viscous correction to the momentum distribution at hadronic freeze-out [**?** **?**]. ~~**[Waiting for $\eta/s(T)$ hydro calculations from Harri Niemi et. al [] and VISH2+1 calculations [?]]**~~

7 Summary

In this article, we report the centrality dependence of correlation between the higher order harmonics (v_3, v_4, v_5) and the lower order harmonics (v_2, v_3) as well as the transverse momentum dependence of v_3-v_2 and v_4-v_2 correlations. The results are obtained by the Symmetric 2-harmonic 4-particle Cumulants (SC)~~method~~. It was demonstrated ~~in the recent ALICE paper~~ earlier in [**?**] that this method is insensitive to the non-flow effects and free from symmetry plane correlations. We have found that fluctuations of ~~v_2-$v_3$and v_3-~~v_2 and v_4-v_3 are anti-correlated in all centralities while fluctuations of ~~v_2-~~v_4~~,~~ ~~v_2-~~v_2, v_5~~and v_3-~~v_2 and v_5-v_3 are correlated for all centralities. This ~~feature was explored to discriminate between various hydro~~ measurement were compared to various hydrodynamic model calculations with different initial conditions as well as different parameterizations of the temperature dependence of η/s. ~~We have~~ It is found that the different order harmonic correlations have different sensitivities to the initial conditions and the system properties. Therefore they have discriminating power ~~on separating the role of the~~ in separating the effects of η/s from the initial conditions to the final state particle anisotropies. ~~Furthermore, the~~ The sign of v_3-v_2 correlation in 0-10% central collisions was found to be different between the data and hydrodynamic model calculations. In the most central collisions the anisotropies originate mainly from fluctuations, ~~i.e.~~ where the initial ellipsoidal geometry ~~characteristic for~~ which is dominating in mid-central collisions plays little role~~in this regime. Hence this~~ . This observation might help to understand the details of the fluctuations in initial conditions. The comparisons to VISH2+1 calculation show that all the models with large η/s regardless of the initial conditions failed to capture the centrality dependence of higher order correlations, more clearly than lower order harmonic correlations. Based on the tested model parameters, the η/s should be small and AMPT initial condition is favored by the data. A quite clear separation of the correlation strength between different initial conditions is observed for these higher order harmonic correlations compared to the lower order harmonic correlations. The default configuration of AMPT model describes well the normalized symmetric cumulants (NSC(m,n)) for most of centralities and for most combinations of harmonics which were considered. Together with the measurements of individual harmonics these results provide further constraints on the system properties and help discriminating between theoretical models. Finally, we have found that v_3 ~~-v_2 and~~ and v_2, v_4 ~~-~~and v_2 correlations have moderate p_{T} dependence in mid-central collisions. This might be an indication of possible viscous corrections for the equilibrium distribution at hadronic freeze-out. The results presented in this article can be used to further optimize model parameters and put better constraints on the initial conditions and the transport properties of nuclear matter in ultra-relativistic heavy-ion collisions.

Acknowledgements

A The ALICE Collaboration